Tellus (2005), 57A, 798–809
Printed in Singapore. All rights reserved

TELLUS

Laboratory observations and simple models of slow oscillations in cooled salt-stratified bodies

By J. A. WHITEHEAD[1]*, LIANKE TE RAA[2], TOMOKI TOZUKA[3], JOSEPH B. KELLER[4] and KEITH BRADLEY[1], [1]*Woods Hole Oceanographic Institution;* [2]*Utrecht University;* [3]*University of Tokyo;* [4]*Stanford University*

(Manuscript received 10 January 2005; in final form 28 April 2005)

ABSTRACT

A laboratory basin of saltwater with a freshwater layer at the top is exposed to cooling from above and inflow of freshwater from a layer that lies alongside. It exhibits oscillations of temperature, salinity, and layer depth when certain parameters are set. A simple analytical model illustrates the basic mechanism. Upon cooling, the layer gradually becomes denser. Ultimately, a density inversion at the interface between the layer and deeper fluid causes a gravitational instability. The layer is mixed with the deeper water and it vanishes. The emplacement of a new thin layer from freshwater inflow at the top repeats the cycle. Layered numerical models duplicate this cycle. Examples incorporate transport of heat out of the top and into the bottom of the layer. In addition, there is salinity transport up through the bottom from turbulent mixing. They reproduce the qualitative structure of the experimental data, but the many simplifications in the model do not permit precise quantitative agreement.

1. Introduction

It is common knowledge among physical oceanographers (Sverdrup et al., 1942) that, although temperature is dominant in determining large-scale ocean density distribution, salinity exerts a steady and pervasive influence. Virtually everywhere in polar oceans, a surface layer 100–300 m deep of lower-salinity water acts as a 'cooling barrier'. Consequently, polar oceans lack widespread deep penetration of dense, newly chilled surface water (deep convection) during winter. Despite this blanketing effect, cold salty water ($<2^{\circ}$C, >35 psu) of polar origin fills all oceans below about 2000 m. The required volume flux of water sinking from the surface to supply this is not trivial, being at least 15×10^6 m^3 s^{-1}. There is extreme sensitivity of deep ocean convection to freshwater presence. Wintertime deep convection is found only in small regions with preferred wind conditions and during cold winters, which combine to make the layer very thin or missing. Examples are known in the Labrador Sea, in the Greenland Sea, within the Gulf of Lyons in the Western Mediterranean Sea, and in the Weddell Sea. In addition, sea-ice growth is strongly retarded in the Arctic when this layer is not present (Bjork et al., 2002) and events characterized by changes in layer salinity of the Arctic Ocean freshwater layer are known (Swift et al., 2005). These could all produce effects upon the large global climate cycles (Broecker et al., 1985; Boyle, 1990; Keigwin and Jones, 1994; Keigwin et al., 1994; Broecker, 1997; Burns et al., 2003).

The sensitivity of ocean convection to salinity distribution produces a number of very large non-linear effects. The first to be understood is the possibility of multiple equilibria. This was pioneered by Stommel (1961) and found independently in an ocean circulation model by Bryan (1986), whose work led to a large number of following studies over the next few years as reviewed by Marotzke (1994) and Whitehead (1995). More recent studies are numerous; some that are more directed to the present study have been made by Manabe and Stouffer (1995), Rahmstorf (1995), Whitehead (1998), Weaver et al. (1999) and Hearn and Sidhu (1999). The second non-linear effect consists of large amplitude non-linear oscillations. A model of such an effect in temperature-salinity systems was pioneered by Welander (1982), and followed by Welander (1986, 1989) and Stommel (1995). In all such cases, either a non-linear equation of state of water was required to produce conditions that allowed the oscillations, or the boundary condition had to be discontinuous, for example by forming and melting ice at the surface (Welander, 1977a,b). In addition, there is a class of rapid oscillations in a loop model, so that a closed circulation cell sped up and slowed down in a balance between fluid inertia and forcing whose phases lead

*Corresponding author.
e-mail: jwhitehead@whoi.edu
Postal address: Department of Physical Oceanography, MS#21 Woods Hole Oceanographic Institution, Woods Hole, MA 02543, USA.

or lag the velocity and thus produce the oscillation (Quon and Ghil, 1995; Dewar and Huang, 1996; Huang and Dewar, 1996). Oscillations have also been found in ocean climate numerical models (Gargett and Ferron, 1996; Zhang et al., 2002; te Raa and Dijkstra, 2002, 2003a,b; te Raa, 2003). In many cases, a simple explanation of the mechanism is lacking. Multiple equilibria and non-linear oscillations are particularly sensitive to the approximations made. For example, Ruddick and Zhang (1989) included internal transport laws for heat and salinity and found an absence of oscillations whereas earlier, simpler models predicted oscillations.

Physical observations of non-linear thermohaline effects in convection are a useful objective to help us understand their contribution to long-term climate variations. Unfortunately, direct ocean observations of either multiple equilibria or non-linear oscillations are presently too limited to provide physical observations of such behavior. To our knowledge, there are no oceanographic observations of either multiple equilibria or non-linear oscillations including data from deep oceans, fjords, marginal seas, and estuaries. Consequently, the only physical observations so far of such effects come from the laboratory (Whitehead, 1996, 1998; Whitehead et al., 2001, 2003; Bulgakov and Skiba, 2003). These laboratory models involved heating a chamber from below that contains freshwater. This is accompanied by a steady inflow of pumped saltwater at some level above the bottom of the chamber. This plume sinks downward from the source and mixes as it descends. The experiments are an inverted model of a polar ocean that we discuss here, which has saltwater that is cooled from above in conjunction with isothermal freshwater flowing in from the side. The observations verify the simple box models. There are two distinctly different equilibrium flow modes. In terms of the polar ocean model, the 'T-mode' is like deep ocean convection in which cold, slightly freshened, rapidly sinking saltwater sinks vigorously to the bottom. The 'S-mode' has colder, fresher water remaining on the surface that flows away at a much slower rate than circulation in the T-mode. However, the 'S-mode' has three layers in the experiments with limited mixing (Bulgakov and Skiba, 2003; Whitehead et al., 2003), a feature not found in the models. The deep salty water is only slightly cooled because the freshwater surface layer acts as a blanket that prevents large cooling of the deeper saltwater. Finally, the flow in each mode was steady except for small convection cells.

2. Laboratory apparatus

The experiment that we report here seems to be the first with observations of slow non-linear oscillations in temperature–salinity driven flows. The apparatus is new (Whitehead and Bradley, 2005), and it is a different design from that described above which revealed multiple equilibria. Two basins are laterally connected by horizontal tubes at the top, middle and bottom, as shown in the sketch in Fig. 1 and the photograph in Fig. 2. The

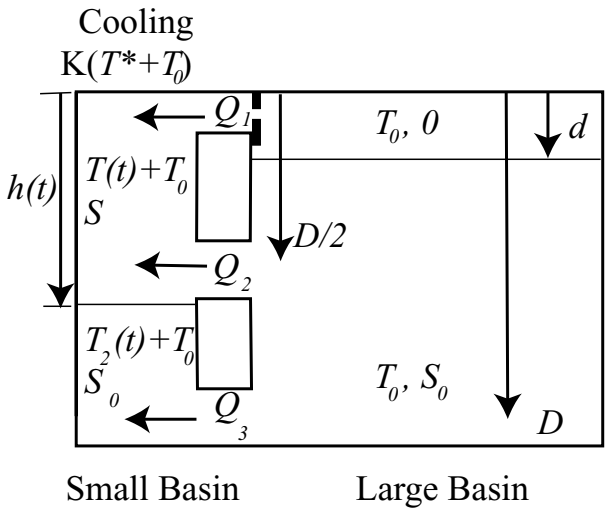

Fig. 1. Elevation view sketch of the configuration discussed in this paper. A large region with a layer of freshwater above salty water lies next to a small basin cooled from above. Three tubes connect the basins at top, middle, and bottom. The layer in the small basin has depth h.

right-hand basin is maintained at temperature T_0 using a radiator. The dyed freshwater layer is held above a saltwater layer with pumps and a drain at the interface depth d, which is above the depth of the middle tube. This basin was designed to provide constant salinity, constant temperature and hydrostatic pressure boundary conditions to the three tubes between the basins. Otherwise, water in this basin is considered to be dynamically passive in spite of the fact that it gives or receives fluid flowing in or out of the three tubes from the small basin.

The left-hand basin is the dynamically active component of the experiment. It is cooled from above with a copper container filled with chilled water at temperature $T^* + T_0$. This basin models a polar sea so T^* is negative. Because the surface layer is cooled from above, the mixed layer deepens from cooling. An inflow of freshwater through the top tube from the right-hand basin to the left introduces freshwater in response to the cooling.

This experimental configuration possesses counterparts to the S- and T-modes. Theory (Whitehead, 2000) predicts that one mode is strongly impeded by salinity changes. We call this the 'fresh-mode', where fresh surface water is slowly drawn into the small basin through the top tube and cooled. It achieves cold temperatures due to the slow inflow. It leaves the small basin through the lower tubes and the water remains fresh. The second mode is called the 'mixed-mode'. Flow in the middle tube reverses direction compared to the fresh mode so that rapid inflow of mid-depth saltwater from the large basin mixes with freshwater entering through the top tube, and the cold mixture exits through the bottom tube. Multiple equilibria and hysteresis are found as T^* is changed. However, the experiments also produce an unanticipated, robust oscillation that we describe here.

3. Experimental method

The experimental apparatus follows the sketch in Fig. 1. It consists of two connected basins. On the right (Fig. 2) is a cubic transparent acrylic plastic large basin of 20-cm sides that have 1 cm thick walls for good thermal insulation. This is connected via three vertically aligned horizontal tubes to a small basin 20 cm high. The small basin is a vertical cylinder with a diameter of 5.1 cm and with 1/2 cm Plexiglas wall thickness to improve thermal insulation. The vertical distance between the centers of the adjacent tubes is 9 cm. The inner radius of the three tubes is 0.95 cm. A thin plate of 1.1 mm thickness is cemented onto the large basin side of the top horizontal tube. It had a hole of 3 mm diameter. The purpose was to increase flow resistance.

The large basin on the right was essentially a source of layered water of constant temperature to the three tubes that fed into the small basin on the left, where the active convection was found. To keep the layers in the large basin at constant salinity values, freshwater at fixed temperature T_0 was pumped into the top of the large basin at a rate of about 0.1 l min^{-1} and a saltwater mixture at the same temperature was pumped into the bottom at the same rate. On the far right, water flowed out through an exit tube 2.5 cm below the water surface, which kept the interface of the two layers sharp. The exit water then ascended within an exit tube to a sharp spillway, where it overflowed and spilled into a drain. In this way, both a free freshwater surface was kept at a fixed elevation, and the submerged exit maintained a sharp interface between the freshwater and the salty water at a depth of $d = 2.5$ cm below the water surface. A heat exchanger in the large basin contained circulating water with temperature T_0 accurate to $\pm$ 0.2°C. The top of the water in the large basin was insulated by a lid of floating Styrofoam. It was found that all experiments maintained the large basin temperature steadily at T_0 with deviation less than $\pm$ 0.5°C.

The small basin on the left exhibited the changes in temperature, and salinity of interest. In addition, cooling from above produced a mixed layer whose depth changed with time. The cooler was a copper cylinder with a vertical axis and with a solid flat circular bottom. This bottom surface was in contact with the water surface in the small basin. The temperature of the water in the cooler was set to $T^* + T_0$ with T^* negative. This is the main variable that expresses the intensity of cooling of the small basin. To minimize heat loss to the room, the average temperature of the experiment was kept close to room temperature by setting T_0 so that for every experiment $(T^* + T_0)/2 =$ 20°C.

The density of the water pumped into the two layers in the large basin on the right apparatus was measured with a densiometer calibrated to one part in 10^5. The freshwater was de-aerated and its density was 998.2 $\pm$ 0.02 kg m^{-3}. The saltwater was a mixture of this freshwater and filtered sea water. It had a density of 1003.4 $\pm$ 0.02 kg m^{-3} at 20°C, giving a density difference between the two layers in the large basin of 5.2 kg m^{-2}. The fact that the salt is not pure sodium chloride is not important. Density

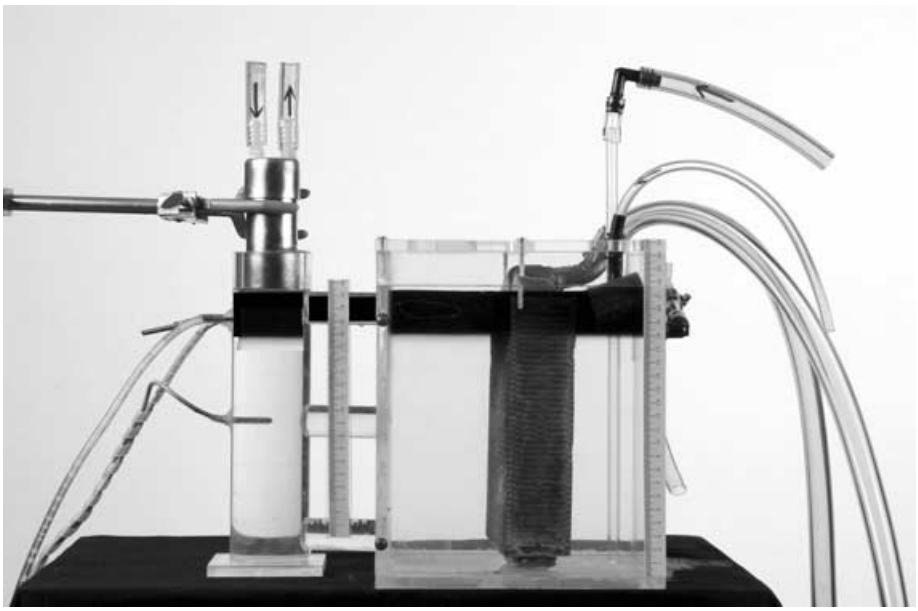

Fig. 2. Side view of the experimental apparatus at the beginning of a run. The small basin on the left is connected to the large basin on the right with three tubes. The freshwater lying in the top of both basins is dyed dark, and the saltwater is clear. Tubes to pump saltwater into the bottom of the large basin and to pump freshwater into the top are on the far right. A radiator in the large basin controls the temperature of both layers. At the top of the small basin on the left is a copper cooler in contact with the water. The two temperature probes are shown on the left at 2.54 cm depth and at 10 cm depth below the top cooler surface. A tube to pump a sample to the densiometer is also visible at 2.54 cm depth. Another tube to return the water to the experiment lies behind this tube.

is almost perfectly linearly proportional to salt concentration for either pure salt or sea salt.

To conduct an experiment, both basins were filled with the two water layers. After this, the freshwater and saltwater pumps were switched on, the temperatures of the control baths were set at the desired values, and the system was left to come to equilibrium. This typically took well over 1 h. Data were subsequently recorded until the run ended.

Both the temperature and the density of the water in the small basin on the left were measured *in situ*. Temperature measurements were made with two permanent probes accurate to $\pm 0.1^{\circ}$C. One temperature probe was 2.5 cm below the top of the water surface in the small basin. The second probe was located 10 cm below the top. The temperature was recorded by each probe once every 15 s. To see the effects of temperature change in the layer upon density, T_0 was subtracted from probe temperature and the result was converted to units of relative density change using a coefficient of thermal expansion of $\alpha = 0.0002$. This value is close to the thermal expansion coefficient of water at 20°C (being only 5% less). The imposed temperature difference $|T^*|$ was as much as 39°C. The density difference between the coldest and warmest water is 5% larger than $|\alpha T^*|$ at this value. For small temperature, the density difference is 5% smaller than $|\alpha T^*|$, so we feel that this value of α is a good first approximation.

To measure water density, water was pumped from a depth of 2.54 cm below the cooling surface in the small basin into a densiometer that reads to four decimal places. Pumping was at a steady rate that was slow enough to allow the sample to reach 20°C there. The density reading was recorded once every 30 s. The water was then returned to the small basin. For analysis of the results, the difference between this density measurement and density of the saltwater in the big reservoir was divided by water density. This is almost exactly linearly proportional to the corresponding salinity difference. The experiments were also viewed by video camera and recorded on videotape.

The oscillations reported here were first discovered in experiments described in te Raa's Fellow's report of the Geophysical Fluid Dynamics (GFD) program for 2001 at http://gfd.whoi.edu/proceedings/2001/vol2001.html. This apparatus was an inverted version of that described here, and the small basin was heated from below with a thin salty layer in the bottom of the big basin. Although the experiment produced reproducible oscillations, proper instrumentation to take time series of temperature and salinity was not available then. Data for those first oscillations are from immersed thermometers and samples withdrawn for manual salinity readings along with video records of the cyclic deepening, mixing away and reformation of the dyed salty layer. In addition, technical problems with condensed air bubbles in the heated water near the small bottom tube were very severe. After another series of experiments that did not eliminate the problems with air bubbles, this configuration was abandoned for the present one.

4. Experimental results

The intensity of the thermal driving is measured by the dimensionless number $-\alpha T^*/\beta S_0$ where $-\alpha T^*$ is the maximum possible density increase from cooling (because $T^* < 0$), and βS_0 is the density difference between the freshwater and saltwater. This is the main variable in the experiments and varies from 0.5 to over 1. Another dimensionless number is tube resistance ratio γ, defined as the top tube flow resistance divided by lower tube flow resistance. The three tube multiple equilibria theory (Whitehead, 2000) shows that for $\gamma < 0.5$, when T^* becomes colder there is a sudden increase of salinity, temperature and heat flux as the fresh mode jumps to the mixed mode. The fresh and mixed modes occupy a range with multiple equilibria. Conversely, for $\gamma \geq 0.5$ multiple equilibria are not found. For this experiment, γ is of the order of 10^{-4}. For practical purposes, this means that the lower half of the small basin has active circulation with the large basin, and to a first approximation one might expect that the salty water in the small basin below the freshwater layer has $T_2 = 0$ and the salinity is S_0. There are other dimensionless numbers that have not yet been greatly varied. Two are given by the ratio of thermal or salinity response times of a layer divided by the time it takes the freshwater layer to flow through the top tube into a small basin and fill it halfway starting with $h = T = S = 0$. Calibration experiments indicate that for a layer of freshwater lying in the small basin, the time-scale for temperature change is about 600 s, and for salinity change (from mixing at the bottom of the layer's interface from convection when the layer is cooled) it is 10^4 s. The time-scale for the layer to fill is 10^3 s. Thus, the former dimensionless number is about 0.6 and the latter is about 10. Other experimental values have not yet been investigated.

Pictures of the new oscillation are shown in Fig. 3. As the layer of dyed freshwater is cooled in the small basin, the depth of the layer slowly increases, and the color decreases by a small amount. Figure 3a shows such a layer after it has thickened. Above it is a new darker layer that has formed at the top. At the base of this new layer is a new internal interface that begins to move downward like the first interface (Fig. 3b). Below this new interface is the old layer, which is now a middle layer. Its color subsequently begins to fade dramatically. We presume that the source of freshwater to the middle layer has been cut off substantially by the formation of the new layer. We see in the videotapes that the water in the bottom of the small basin begins to darken and we interpret this as showing increased transport of freshwater from the middle layer into the bottom layer. This implies that there is also increased transport of saltwater from the bottom layer into the middle layer, which is consistent with the fading of color of the middle layer. After some time interval, the interface below the middle layer begins to exhibit large vertical excursions and waves sometimes break. The large excursions become greater and more frequent with time. As time progresses, the interfacial waves in the lower interface break more frequently and the color difference between the lower layer and the fluid

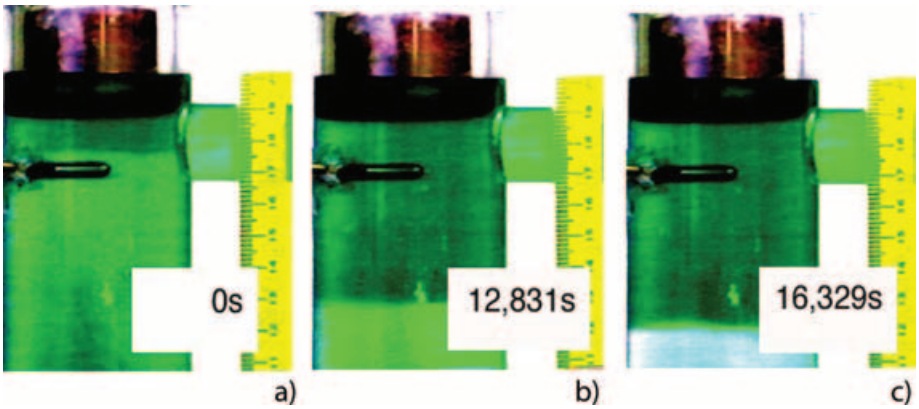

Fig. 3. (a) Close-up of a new layer forming at the top of the small basin. The white box shows running time in seconds for this and the next two panels. (b) The layer has deepened after about 3.5 h. (c) The old layer at the bottom has overturned and mixed away about an hour later.

below it becomes much fainter. Suddenly (within about 5 min, as compared to a few hours for the entire cycle to occur) the bottom interface mixes away by direct overturning. The middle layer vanishes and only the upper interface is left (Fig. 3c). The new freshwater layer in the small basin deepens with time. Eventually another new layer forms at the surface of the cooled layer as in Fig. 3a and this repeats the cycle.

Temperature and salinity records (Fig. 4a) show a migration back and forth between the fresh-mode and the mixed-mode. Results from over 400 h of experimental running time revealed oscillations for $-\alpha T^*/\beta S_0 < 1.2$. There is a small range where this overlaps the steady fresh mode, which is found for $1.35 > -\alpha T^*/\beta S_0 > 1.15$. Also, the steady mixed mode is found for $-\alpha T^*/\beta S_0 > 1.2$. The ranges of the steady flow and a comparison with steady theory are given by Whitehead and Bradley 2005.

Records of oscillations for three different experiments are shown in Figs. 4a–c for which $-\alpha T^*/\beta S_0 = 0.5, 0.85$ and 1.15 respectively. The first case (Fig. 4a) corresponds to the smallest temperature difference in all the experiments for which we acquired a sufficiently long time series. The cold driving temperature was $T^* = -18^\circ$C. We will describe the cycle starting from the initial time shown in this figure, although the actual experiment was started earlier. At the beginning, there was a thin layer near the top of the small basin. The thickness of this layer increased with time. After about 10^4 s, the interface separating this layer from the fluid below, which defines the bottom of this layer, reached the middle tube where the lower temperature probe was located. The letter 'M' in Fig. 4a indicates that the interface reached the middle tube and that T_{middle} suddenly decreases. The temperature probe next to the middle tube recorded a rapid decrease in temperature as the interface passed the probe. This passage brought colder and fresher water to that depth and the top and middle probes had almost the same temperature after this.

Somewhat later, a new layer formed at the top of the small basin. The letter 'F' in Fig. 4a indicates this formation event. The temperature of the top probe suddenly became much colder, which signified that that the new layer passed the top probe and the layer was colder than the fluid below. Later, at about 3.8×10^4 s, the bottom layer overturned and mixed with the fluid below it. The letter 'O' in Fig. 4a indicates this. Before this happened, the bottom interface exhibited increasingly large vertical excursions in the videotape movies taken of the experiment. The mixing and disappearance of the bottom layer completes one cycle. Thereafter, the upper layer is the only one present and the cycle repeats itself.

Figure 4b shows a more rapid oscillation driven by $T^* = -22^\circ$C. In this case, the bottom temperature probe was 2.5 cm below the top probe rather than at the middle tube. The data from the bottom probe are shown as dots. The interface started from the top and descended rapidly through the level of the top probe. At about 10^3 s later, the interface descended through the level of the bottom probe. As the layer continued to descend, both temperature and salinity increased in the top layer. Suddenly at about 0.5×10^4 s another layer began to form at the top. This produced the plateau in the T and S curves in the figure. Then at about 0.8×10^4 s the bottom layer overturned and mixed away, leaving only the top layer to start a new cycle.

Figure 4c shows one of the most rapid oscillations with $T^* = -30^\circ$C. The interface never got close to the middle tube before it overturned and mixed away. As the interface was descending, temperature and salinity of the layer increased rapidly. Another layer was not visible before the bottom interface mixed away. Instead after the layer mixed away, the freshwater flowed in through the top tube to start a new layer.

The oscillation periods of all experiments are shown in Fig. 5. This includes data from the GFD report by te Raa in 2001, which is called set 1, and data from another series of experiments, called set 3. The set 3 apparatus is identical to the apparatus described

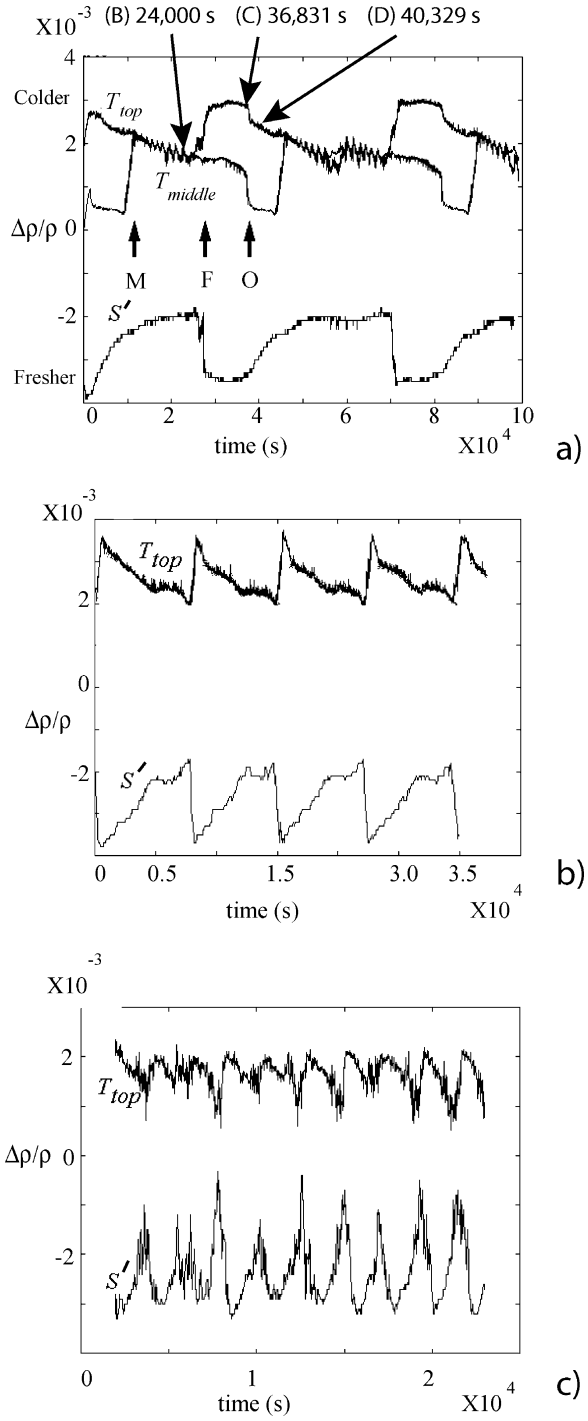

Fig. 4. Time series of density due to temperature and to salinity for three values of cooling temperature. (a) The top two curves, labeled 'T_{top}' and 'T_{middle}', respectively, are values of $-\alpha T$ from probes 2.54 and 10.0 cm below the top. The density due to layer salinity is represented using $\beta(S - S_0)$. This curve is indicated by 'S''. The value is negative, because the water in the layer is fresher than the deep right-hand basin water of salinity S_0. The forcing strength is (a) $-\alpha T^*/\beta S_0 = 0.5$. (b) $-\alpha T^*/\beta S_0 = 0.85$. (c) $-\alpha T^*/\beta S_0 = 1.15$.

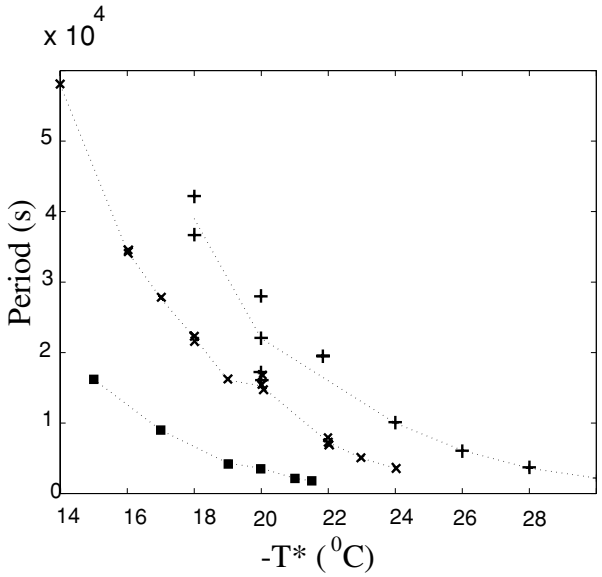

Fig. 5. Period of oscillation for all three sets. Squares, set 1; *x*, set 3; +, set 4.

here (set 4) except that the top tube was 3.5 cm long rather than a hole in a plate. However, the tube had the same diameter as the hole in the plate. Set 3 experiments produced a number of oscillating flows that existed for many cycle periods. Unfortunately, although videotapes were obtained along with temperature time series records, we did not record salinity time series in set 3. Thus, no other data from set 3 are shown in this paper. The period for each oscillation was measured from either the top or the bottom temperature probe data by noting the time interval for the temperature of the top probe to cross its mean twice (up and down again) or from videotapes. The periods are very long for small values of cooling and the period becomes much shorter with greater cooling. No cycles are exactly periodic, and periods have considerable range about their mean value. Using a value for thermal diffusivity of water of 1.4×10^{-7} m^2 s^{-1}, we estimate that the thermal relaxation time d^2/κ for a 1 cm deep layer would be about 1.4×10^3 s, and for 10 times greater depth would be about 1.4×10^5 s. So, almost all the periods shown in Fig. 5 span these two time-scales.

5. An anaytic model

The experimentally observed periodic motion appears to be a typical relaxation oscillation. There is a relatively long time interval, of duration t_1, during which the upper layer gradually deepens and becomes cooler and denser. This is the interval during which the gravitational potential energy of the system increases. Ultimately, the density of the upper layer equals that of the lower layer and begins to exceed it. Then the system becomes unstably stratified. In a short interval, of duration t_2, it overturns, mixing the upper layer with the lower layer and returning the system to

a stable state. A new upper layer is formed and then this cycle repeats.

To describe the oscillation analytically, we consider a layer of freshwater of depth $h(t)$, uniform temperature $T_0 + T(t)$ and cross-sectional area A. It lies above deep saltwater of temperature T_0 and salinity S_0. Freshwater of temperature T_0 flows into the layer at the volume flux rate $Q_1 = Aw$ so that the layer deepens at the rate w. Thus, its depth at time t is $h(t) = h_i + wt$, where h_i is its initial depth. In addition, the layer is cooled from above at the rate $k(T^* - T)/d_0$, where $T^* + T_0$ is the coolant temperature, k is the thermal conductivity, and d_0 is thickness of the material between coolant and the top of the layer of water. The cooling produces cellular convection within the layer that will keep the layer well mixed.

Using Fig. 1, the configuration can be visualized as being a case with $h \ll D/2$. Also, the bottom two tubes are so large that the deep fluid is very effectively flushed by buoyant circulation through the bottom two tubes as it is cooled by conduction with the cooler layer above it. In this way, $T_2 \ll T$, so we set $T_2 = 0$. In addition, mixing of salt from the lower fluid to the upper layer across the interface is neglected, so $S = 0$.

Assuming for simplicity that the layer is not receiving any heat or salt through the bottom of the layer, its temperature change is governed by the energy conservation equation

$$\frac{\mathrm{d}}{\mathrm{d}t}\rho_0 C_p h T = k(T^* - T)/d_0. \tag{5.1}$$

Here C_p is the specific heat of water at constant pressure, ρ_0 is the water density at temperature T_0 and salinity $S = 0$, and the small variation of ρ with T is neglected. With $h(t) = h_i + wt$, this energy equation becomes a first-order ordinary differential equation for $T(t)$. Its solution, with the initial condition $T(0) = T_i$, is

$$T(t) = T_f + (T_i - T_f)\left(1 + \frac{wt}{h_0}\right)^{-1-a} \tag{5.2}$$

where $a = k/d_0\ \rho_0\ C_p$ and $T_f = aT^*/(1 + a)$.

As t increases from zero, $T(t)$ tends toward T_f. When T_f is less than T_i the layer cools and its density $\rho = \rho_0\ (1 + \beta S - \alpha T) = \rho_0\ (1 - \alpha T)$ increases. The density of the deep salty water below it is $\rho = \rho_0\ (1 + \beta S_0)$. If $-\alpha T_f < \beta S_0$, the upper layer density never reaches that of the deep water and the layer depth grows forever. However, if $-\alpha T_f > \beta S_0$ there will be a time t_1 when the upper layer density equals that of the deep water and overturning begins. This happens when $-\alpha T = \beta S_0$. Using eq. (5.2) for $T(t_1)$ in this equation, and solving for t_1 yields

$$t_1 = \left[\left(\frac{T_f - T_i}{T_f + (\beta S_0/\alpha)}\right)^{1/(1+a)} - 1\right]\frac{h_i}{w}. \tag{5.3}$$

We suppose that after t_1 overturning occurs during an interval of duration t_2. While overturning and mixing away of the upper layer occurs, the incoming flow deposits a new layer of freshwater, of depth $h_i = wt_2$, on top of the mixed water column. Then the process begins again. It repeats periodically with period

$$t_1 + t_2 = \left[\frac{T_f - T_i}{T_f + (\beta S_0/\alpha)}\right]^{1/(1+a)} t_2. \tag{5.4}$$

The model cannot determine the length t_2 of the short interval of mixing and of deposition of the new upper layer. To do this would require a model of the mixing process, and of the formation of the new upper layer. However, the model does determine the duration t_1, of the long build-up period in terms of the initial depth of the upper layer.

In this model we keep the inflow rate w = constant for simplicity. In the laboratory, and in the numerical calculations with mixing at the base of the layer, the emplacement of a new layer is accompanied by a faster inflow of freshwater. Thereafter, the inflow slows down significantly during the long time interval when the layer is deepening, becoming salty and cooling.

Although this model could be used to estimate oscillation periods for the experiments by using eq. (5.4) along with some estimate of inflow velocities, we have chosen not to do this. There are too many approximations made compared to the actual experiment. For example, there is no mixing of both salinity and heat at the bottom of the interface in this model. Also, the cooling coefficient is not really completely constant in the experiment, and the inflow is by no means constant. Instead, the numerical models in the following section retain such processes as the next step toward a complete model of the experiment.

6. Numerical models

We use conservation equations for water, heat and salt to calculate the evolution of temperature and salinity of a layer. To determine freshwater flowing into the top through the top tube, we use an inviscid flow law. A scaling analysis indicates that the top tube hole is so short that no boundary layer can develop along the tube. Consequently, for the inflow of freshwater through the small tube next to the top layer, we will use Bernoulli's law in the form $u^2/2 = -g\eta$, where η is the difference in surface elevation between the large and small basin. In all cases, this is negative. If we assume that hydrostatic pressure at the base of the layer in the small basin is equal to pressure at that same elevation in the large basin, then the relation $g(\eta + h)(1 + \beta S - \alpha T) = g(h + \beta S_0\ (h - d))$ determines η. Equating volume flux through the top tube to change in depth of the layer and using the Boussinesq approximations, ($\beta S \ll 1$, $-\alpha T \ll 1$),

$$\frac{\mathrm{d}h}{\mathrm{d}t} = \frac{a}{A}\sqrt{-2g((\beta(S_0 - S) + \alpha T)h - \beta S_0 d)} \tag{6.1}$$

where a is area of the top tube.

For the heat flow equation of the layer, we use a simple layer model

$$\frac{\mathrm{d}hT}{\mathrm{d}t} = W_{uT}(T^* - T) - W_{lT}T. \tag{6.2}$$

Physically the exchange coefficients W with subscripts should not be confused with a unidirectional flow. Instead they might be pictured as an exchange flow of warmer fluid up and colder fluid down across an interface, each with average velocity W. The meaning of the subscripts in the coefficients is as follows. The subscript u indicates that this is for the upper boundary, the subscript l for the lower boundary, and subscript T indicates that this is for heat flux. If W_{uT} is a constant value and layer depth is constant, this formulation is a relaxation condition (Haney, 1971) widely used in numerical modeling. The salinity obeys

$$\frac{\mathrm{d}hS}{\mathrm{d}t} = W_{lS}(S_0 - S). \tag{6.3}$$

with subscript 'S' for a salt flux through the lower boundary from turbulent mixing by the convection that is produced by heat transport upward through the layer. To estimate W_{uT} we assume that the copper surface that lies above the layer of freshwater in the small basin is at the temperature of the cold-water bath, and estimate heat transport by cellular convection cooled from above. The formula for heat transport from cellular convection between two horizontal boundaries is

$$H = k\Delta T Nu/\delta, \tag{6.4}$$

where k is the thermal conductivity of water, ΔT is temperature difference between a top rigid boundary and the bottom rigid boundary, and δ is the layer thickness. The Nusselt number expresses the enhancement of heat flux by Rayleigh–Benard convection. Siggia (1994) gives the simplest empirical formula for the Nusselt number to be

$$Nu = 0.06Ra^{1/3} \tag{6.5}$$

for Rayleigh–Benard convection between rigid boundaries where the Rayleigh number is

$$Ra = g\alpha\Delta T\delta^3/\kappa\nu. \tag{6.6}$$

Here, g is acceleration of gravity, $\kappa = k/\rho_0\, C_p$ is the thermal diffusivity of water with the constants defined in Section 5, and ν is viscous diffusivity of water. The range of validity for eq. (6.5) is $Ra = 10^5$–10^6 for a liquid with Prandtl number ν/κ from 2 to 10, which holds for the mixed layer in the present experiment. The mixed layer corresponds to the upper half of the cellular convection layer, so that $T^* - T = 0.5\Delta T$. This must be used along with an estimate of heat loss through the sidewalls. The layer is warmed considerably because the insulating effect of the Plexiglas allows considerable warming of the cold layer from the room. We estimate that for every unit of cooling received by the mixed layer, about 70% is warmed by the room. Thus, we assign an efficiency of only 30% to the convection and produce an estimate of heat flow that cools the layer

$$H = \rho C_p W_{uT}(T - T^*) \tag{6.7}$$

with

$$W_{uT} = 0.024\left[\frac{-g\alpha(T^* - T)\kappa^2}{\nu}\right]^{1/3}. \tag{6.8}$$

We also require heat and salt transport through the lower interface of the layer in this model. Heat enters the bottom of the freshwater layer by thermal conduction through the thermal boundary layer of the interface between the two layers. The convective exchange across the lower interface also mixes salinity into the freshwater layer. To quantify the flux of heat and salinity, appropriate formulae are known from laboratory measurements. Huppert (1971) (see Turner, 1973, eq. 8.3.4) gives a formula based on laboratory data for the ratio of heat flow through a salt stratified interface to the same value for flux through a rigid boundary. In our notation, this is

$$W_{lT} = 3.8W_{uT}R_\rho^{-2} \tag{6.9}$$

where

$$R_\rho = \frac{\beta(S_0 - S)}{-\alpha T}$$

is called the 'density ratio'. It is the ratio of the magnitude of density change due to the salinity difference across the interface to the density change due to temperature difference. Next, we need a formula for salinity transport. There are two formulae for 'lower salt flux exchange velocity' depending on the value of R_ρ. Inspection of two straight lines in fig. 8.15 of Turner (1973) gives the two formulae:

$$W_{lS} = 0.15W_{lT} \quad \text{for} \quad R_\rho > 2 \tag{6.10}$$

or

$$W_{lS} = [1.85 - 0.85R_\rho]W_{lT} \quad \text{for} \quad 1 < R_\rho \leq 2. \tag{6.11}$$

Finally, at $R_\rho = 1$ the layer mixes away.

Equations (6.1)–(6.3) were numerically integrated forward in time using eqs. (6.8), (6.9) and (6.10) or (6.11) and assuming $T_2 = 0$. The calculations used the following values for the constants: $g = 9.8$ m s^{-1}, $\beta S_0 = 0.0052$, $\kappa = 1.4 \times 10^{-7}$ m^2 s^{-1}, $\nu = 10^{-6}$ m^2 s^{-1}, $\alpha = 2 \times 10^{-4}\,^\circ$C, and $a/A = 3.5 \times 10^{-3}$. The cold temperature T^* is specified for each run. Although the experiments start with a stagnant freshwater layer in the small basin with zero depth, in this model the early evolution of the layer is ignored and the calculations start with a layer with $h = d$. Also, for a new layer we set $T = S = 0$. As time progresses, temperature, salinity, and depth of the layer changes. If the layer reaches a value of $R_\rho = 1$, we let the layer vanish away (as it would by mixing) and a new layer with the same starting conditions as before replaces the layer.

Calculations reveal that below a critical value of $\alpha T^*/\beta S_0 = 0.15$ the layer grows in thickness indefinitely. The layer density approaches a steady value because it never achieves greater density than the fluid below it. This regime is also found in the simple analytical model in Section 5. This state is closest to a steady

regime in the experiments in which the layer remained lighter than the deep fluid. In those experiments the layer thickness growth was terminated by exchange flow through the middle tube. The steady flow results for the experiments are reported by Whitehead and Bradley 2005. Above the critical value of $\alpha T^*/\beta S_0 = 0.15$, oscillations were found.

Three examples of the oscillations are shown in the three panels in Fig. 6. In all three cases the numerical oscillations qualitatively resemble those in the experiments. In Fig. 6a, the shape of the theoretical curves is roughly the same as the experimental curves, but this is less so in Figs. 6b and c. The period of the oscillation varies inversely with T^* as in the experiments. Quantitatively, there are some close correspondences. Temperature amplitude is roughly 10^{-3} in both model and experiment. However, in the numerical model the salinity amplitude is tens of percent larger and the periods of oscillation are tens of percent shorter than in the experiment.

Other numerical calculations are described in a GFD program Fellow's report by Tozuka (see http://gfd.whoi.edu/proceedings/2002/vol2002.html). They use equations for flow in a three-tube geometry like the laboratory experiment. In these, heat and salt transport was included in the bottom of the mixed layer and the temperature below the mixed layer T_2 was allowed to change. Salt and temperature transport at the base of the mixed layer was provided by a Kraus–Turner parametrization (Kraus and Turner, 1967). Over a wide range of parameters there were regions in parameter space with no oscillation. This is typical behavior for such oscillators. In addition, there were two regions with two distinct types of oscillation. Two distinct oscillation types is not typical of simple relaxation oscillators, and it is clearly linked to the fact that the excursions of the interface had different roles in the two types. In one case, the layer interface reached the bottom of the basin during part of the cycle. In the other, the same was not true.

We show one example of the first type of oscillation in Fig. 7. This is for a case with $W_{uT}/a\sqrt{2g\beta S_0} = 0.5$ and an upper layer depth divided by tank depth of 0.03. The middle tube is not at mid-level in this case and its depth divided by tank depth is 0.3. The ratio of upper tube flow resistance to middle or bottom tube resistance is 1.0. The temperature unit is divided by $\beta S_0/\alpha$ and the salinity unit is divided by S_0. The time-scale is $AD/a\sqrt{2g\beta S_0}$.

At $\tilde{t} = 4.3$ the upper layer starts to grow. The upper layer temperature T_1 decreases rapidly due to surface cooling while the salinity of the layer S_1 increases due to entrainment of bottom water into the layer by mixing. Then, at $\tilde{t} = 5$ the interface descends below the middle tube. Warm and salty water from the large basin flows into the upper layer of the small basin causing T_1 to initially increase and S_1 to continue to increase steadily. At $\tilde{t} = 7.8$ the interface reaches the bottom of the small basin and there is only one layer in the small basin. Shortly thereafter, at $\tilde{t} = 8.1$ the condition for the formation of a new layer is satisfied and a new layer forms and starts to grow, completing the cycle.

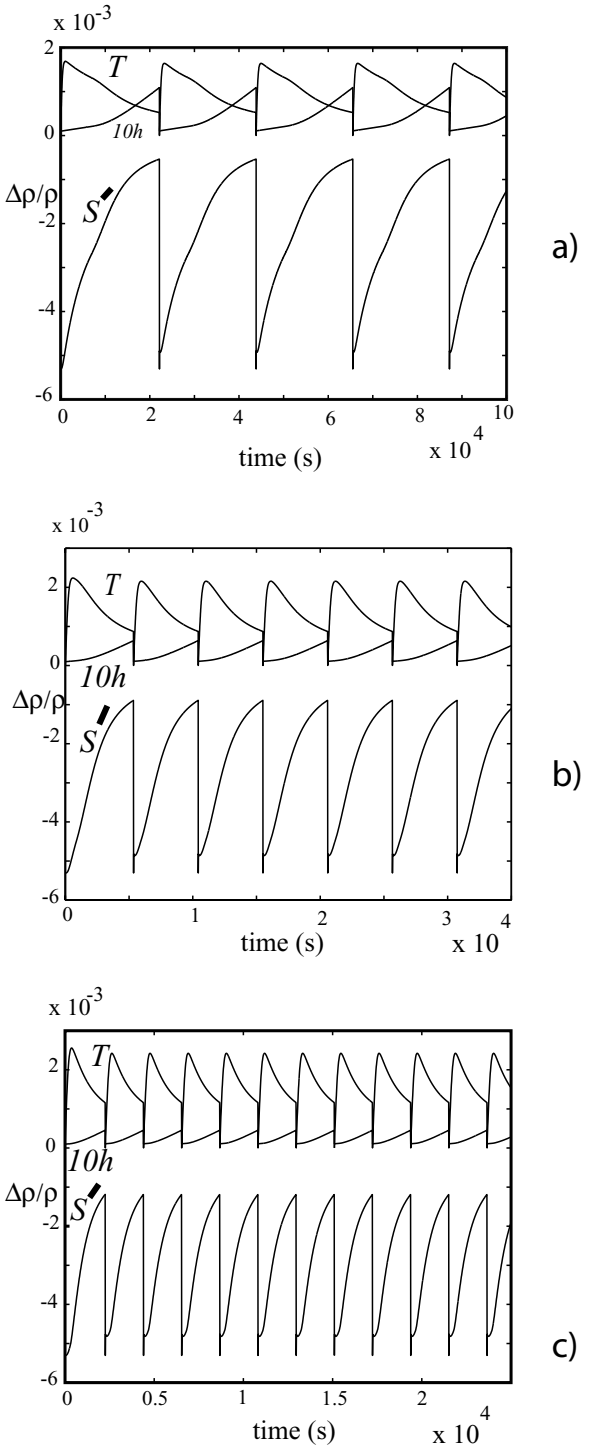

Fig. 6. Time series of density and layer depth from numerical calculations. Density from temperature and salinity are given in the same units as in Fig. 4. Also included is layer depth h. Units for depth are multiplied by 10 and given in meters. This stretches the vertical scale and makes the value of depth more visible. Parameters are made to be as close to those for the laboratory runs in Fig. 4. (a) $-\alpha T^*/\beta S_0 = 0.5$ (b) $-\alpha T^*/\beta S_0 = 0.85$. (c) $-\alpha T^*/\beta S_0 = 1.15$.

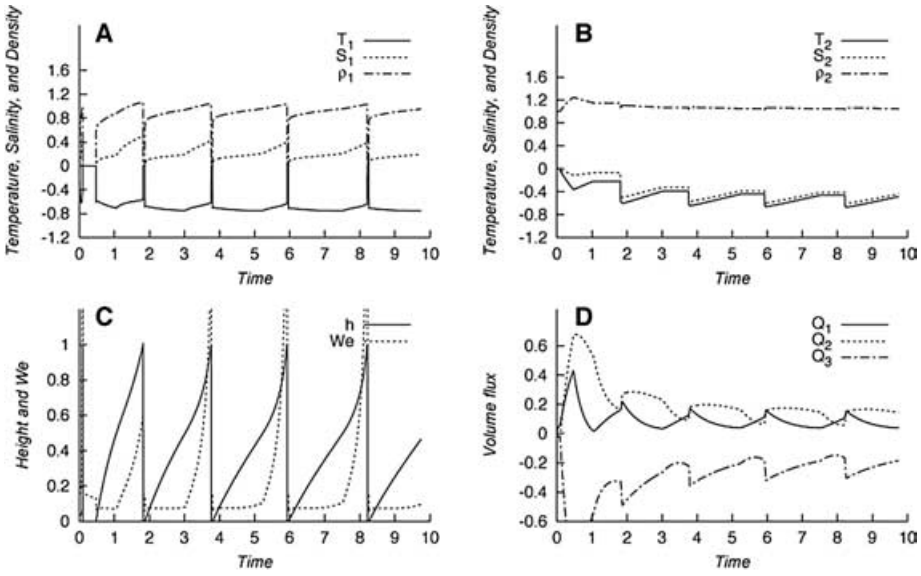

Fig. 7. Results of calculations using more general equations. Forcing strength is $-\alpha T^*/\beta S_0 = 1.0$ (a) Temperature, salinity and density change of the top layer. Subscript 1 refers to properties in the top mixed layer in the left-hand basin. (b) Temperature, salinity and density change of water below the mixed layer in the left-hand basin. Subscript 2 refers to those properties under that layer in the left-hand basin. (c) Layer depth and vertical velocity of the interface in the left-hand basin. (d) Volume flux through the three tubes. The symbol Q_i is for volume flux through a tube with subscript $i = 1, 2, 3$ starting from the top.

7. Discussion

In the laboratory and in the numerical calculations with mixing at the base of the layer, the mechanism for a typical oscillation seems quite clear. The emplacement of a new layer is accompanied by a faster inflow of freshwater. Thereafter, the inflow slows down significantly during the long time interval when the layer is deepening, during which time the layer becomes salty and colder. Finally, the layer overturns and the cycle repeats itself with a new rapid inflow. In the ocean, such a cycle would be characterized by an interval of rapid freshening separated by a gradual increase of salinity of the surface layer through time. Eventually the surface layer ceases to exist as a barrier to deep convection and surface water mixes into the interior during winter. A new rapid inflow of freshwater re-establishes the surface layer.

The edge of the freshwater layer in the Arctic Ocean is known to move around (Bjork et al., 2002), so the concept of a freshwater layer present or not present in one location is in qualitative agreement with observations. In addition, the salinity of the surface layer in the Arctic is known to have increased in the mid-1970s (Swift et al., 2005). Many mechanisms are possible causes for this such as wind driven surface divergence in addition to convective mixing with deeper salty water, which was clearly important in these experiments. In natural bodies such as bays, fjords, or even in large Arctic or Antarctic regions, oscillations like these could possibly exist with periods given by temperature and freshwater storage times. Thus, they may exist with periods of months, years, tens of years, or even over centuries.

We close by noting that in other problems in metallurgy, volcanology, limnology with dissolved gases, and engineering if a multicomponent fluid flows into a region with temperature or pressure change so that one component condenses or crystallizes, similar bulk equations can exist (Batchelor et al., 2001). In such cases, a surface mixed layer of some compositional difference with deeper fluid might gradually mix downward from cooling and mix away and then be replaced by a new layer. The same can happen in an inverted circumstance, by intruding salty water in conjunction from heating from below. A layer of hot denser material might come in and slowly mix up as it is cooled by both the walls and by ambient fluid. Then, this layer will be replaced by a new dense layer, which repeats the cycle. Indeed, our exploratory experiments by te Raa (http://gfd.whoi.edu/proceedings/2001/vol2001.html) had this configuration and the physical processes can have the same features even though certain signs are reversed in the governing equations.

8. Acknowledgments

Support for the laboratory experiments was provided by the National Science Foundation, Physical Oceanography Section, under Grant OCE 00-81179. Support for the Geophysical Fluid Dynamics Study Program was provided under Grant OCE 98-10647 and the Office of Naval Research under Grant N00014-97-1-0934. Support for part of the laboratory work of JAW was supported by the Paul M. Fye Chair of the Woods Hole Oceanographic Institution. The help of Jeanne Fleming is also gratefully

acknowledged. Woods Hole Oceanographic Institution contribution number 11325.

References

Batchelor, G. K., Moffatt, H. K. and Worcester, M. G. (Eds) 2001. *Perspectives in Fluid Dynamics: A Collective Introduction to Current Research*, Cambridge University Press, Cambridge, 646 pp.

Bjork, G., Soderkvist, J., Winsor, P., Nikolopoulos, A. and Steele, M. 2002. Return of the cold halocline layer to the Amundsen Basin of the Arctic Ocean; Implications for the sea ice mass balance. *Geophys. Res. Lett.* **29**, 10.1029/2001GL014157.

Boyle, E. A. 1990. Quaternary deepwater paleooceanography. *Science* **249**, 863–870.

Broecker, W. S. 1997. Thermohaline circulation, the Achilles heel of our climate system: will man-made CO_2 upset the current balance? *Science* **278**, 1582–1588.

Broecker, W. R., Peteet, D. M. and Rind, D. 1985. Does the ocean–atmosphere system have more than one stable mode of operation? *Nature* **315**, 21–26.

Bryan, F. 1986. High-latitude salinity effects and interhemispheric thermohaline circulations. *Nature* **323**, 301–304.

Bulgakov, S. N. and Skiba, Y. N. 2003. Are transitions abrupt in Stommel's thermohaline box model? *Atmosfera* **16**, 205–229.

Burns, S. J., Fleitmann, D., Matter, A., Kramers, J. and Al-Subbary, A. A. 2003. Indian Ocean climate and an absolute chronology over Dansgaard/Oeschger events 9 and 13. *Science* **201**, 1365–1367.

Dewar, W. K. and Huang, R. X. 1996. On the forced flow of salty water in a loop. *Phys. Fluids* **8**, 954–970.

Gargett, A. E. and Ferron, B. 1996. The effects of differential vertical diffusion of T and S in a box model of thermohaline circulation. *J. Marine Res.* **54**, 827–866.

Haney, R. 1971. Surface thermal condition for ocean circulation models. *J. Phys. Oceanography* **1**, 241–248.

Hearn, C. J. and Sidhu, H. S. 1999. The Stommel model of shallow coastal basins. *Proceedings of the Royal Society of London A* **455**, 3997–4011.

Huang, R. X., and Dewar, W. K. 1996. Haline circulation: bifurcation and chaos. *J. Phys. Oceanography* **26**, 2093–2106.

Huppert, H. 1971. On the stability of a series of double-diffusive layers. *Deep-Sea Res.* **18**, 1005–21.

Keigwin, L. D. and Jones, G. A. 1994. Western North-Atlantic evidence for millennial-scale changes in ocean circulation and climate. *J. Geophys. Res.* **99**(C6), 12 397–12 410.

Keigwin, L. D., Curry, W. B., Lehman, S. J. and Johnsen, S. 1994. The role of the deep-ocean in North-Atlantic climate-change between 70-Kyr and 130-Kyr ago. *Nature* **371**, 323–326.

Kraus, E. B. and Turner, J. S. 1967. A one-dimensional model of the seasonal thermocline II: the general theory and its consequences. *Tellus* **19**, 98–106.

Manabe, S. and Stouffer, R. J. 1995. Simulation of abrupt climate change induced by freshwater input to the North Atlantic Ocean. *Nature* **378**, 165–167.

Marotzke, J. 1994. Ocean models in climate problems. In: *Ocean Processes in Climate Dynamics; Global and Mediterranean Examples.* (eds. P. Malanotte-Rizzoli, and A. R. Robinson). Kluwer, Dordrecht, 437 pp.

Quon, C. and Ghil, M. 1995. Multiple equilibria and stable oscillations in thermosolutal convection at small aspect ratio. *J. Fluid Mech.* **291**, 33–56.

Rahmstorf, S. 1995. Bifurcations of the Atlantic thermohaline circulation in response to changes in the hydrological cycle. *Nature* **378**, 145–149.

Ruddick, B. J. and Zhang, L. 1989. The mythical thermohalineoscillator? *J. Marine Res.* **47**, 717–746.

Siggia, E. D. 1994. High Rayleigh Number Convection. *Ann. Rev. Fluid Mech.* **25**, 137–168.

Stommel, H. 1961. Thermohaline convection with two stable regimes of flow. *Tellus* **13**, 224.

Stommel, H. 1995. A thermohaline oscillator. In: *Collected Works of Henry M. Stommel, II* (eds. N. Hogg, and R. X. Huang). Am. Meteorol. Soc., Boston, MA, 648–649.

Swift, J. H., Aagaard, K., Timokhov, L. and Nikiforov, E. G. 2005. Long-term variability of Arctic Ocean Waters: wvidence from a reanalysis of the EWG data set. *J. Geophys. Res.* in press.

Sverdrup, H. U., Johnson, M. W. and Fleming, R. H. 1942. *The Oceans*. Prentice-Hall, Englewood Cliffs, NJ, 1087 pp.

te Raa, L. A. 2003. Internal variability of the thermohaline ocean circulation, PhD thesis, Utrecht University, the Netherlands.

te Raa, L. A. and Dijkstra, H. A. 2002. Instability of the thermohaline ocean circulation on interdecadal time scales. *J. Phys. Oceanogr.* **32**, 138–160.

te Raa, L. A. and Dijkstra, H. A. 2003a. Sensitivity of North-Atlantic multidecadal variability to freshwater flux forcing. *J. Climate* **16**, 2586–2601.

te Raa, L. A. and Dijkstra, H. A. 2003b. Modes of internal thermohaline variability in a single-hemispheric ocean basin. *J. Marine Res.* **61**, 491–516.

Turner, J. S. 1973. *Buoyancy Effects in Fluids*. Cambridge University Press, Cambridge, 367 pp.

Weaver, A. J. Bitz, C. M., Fanning, A. F. and Holland, M. M. 1999. Thermohaline circulation: high-latitude phenomena and the difference between the Pacific and Atlantic. *Ann. Rev. Earth and Planet. Sci.* **27**, 231–285.

Welander, P. 1977a. Thermal Oscillation in a fluid heated from below and cooled to freezing from above. *Dyn. Atmos. Oceans* **1**, 215–223.

Welander, P. 1977b. Observations of oscillatory ice states in the simple convection experiment. *J. Geophys. Res.* **82**, 2591–2592.

Welander, P. 1982. A simple heat-salt oscillator. *Dyn. Atmos. Oceans* **6**, 233–242.

Welander, P. 1986. Thermohaline effects in the ocean circulation and related simple models. In: *Large-Scale Transport Processes in Oceansand Atmospheres* (eds, J. Willebrand, and D. L. T. Anderson). D. Reidel, Dordrecht, 163–200.

Welander, P. 1989. A new type of double diffusive instability. *Tellus* **41A**, 66–72.

Whitehead, J. A. 1995. Thermohaline ocean processes and models. *Ann. Rev. Fluid Mech.* **27**, 89–114.

Whitehead, J. A. 1996. Multiple States in doubly-driven flow. *Physica D* **97**, 311–321.

Whitehead, J. A. 1998. Multiple T–S states for estuaries, shelves and marginal seas. *Estuaries* **21**, 278–290.

Whitehead, J. A. 2000. Stratified convection with multiple states. *Ocean Modelling* **2**, 109–121.

Whitehead, J. A. and Bradley, K. 2005. Laboratory studies of stratified convection with multiple states, Ocean Modeling, in press.

Whitehead, J. A., Lawson, W. G. and Salzig, J. 2001. Multistate flow devices for geophysical fluid dynamics and climate. *Am. J. Phys.* **69**, 546–553.

Whitehead, J. A., Timmermans, M. L. E., Lawson, W. G., Bulgakov, S. N., Zatarian, A. M. and co-authors. 2003. Laboratory studies of thermally and/or salinity-driven flows with partial mixing. Part 1: Stommel transitions and multiple flow states. *J. Geophys. Res.* **108**, 3036 (doi:10.1029/2001JC000902).

Zhang, R., Follows, M. and Marshall, J. 2002. Mechanisms and thermohaline mode switching with application to warm equable climates. *J. Climate.* **15**, 2056–2070.